HHS Public Access

Author manuscript

J Neurooncol. Author manuscript; available in PMC 2017 March 01.

Published in final edited form as:

J Neurooncol. 2016 March ; 127(1): 33–41. doi:10.1007/s11060-015-2022-8.

Quantitative imaging of magnesium distribution at single-cell resolution in brain tumors and infiltrating tumor cells with secondary ion mass spectrometry (SIMS)

Subhash Chandra[1,*], **Dylan J. Parker**[1], **Rolf F. Barth**[2], and **Susan C. Pannullo**[3]

[1]Department of Biomedical Engineering, Cornell University, Ithaca, NY 14853, U.S.A

[2]Department of Pathology, The Ohio State University, Columbus, OH 43210, U.S.A

[3]Weill Cornell Brain and Spine Center, 1305 York Avenue, New York, NY 10021, U.S.A

Abstract

Glioblastoma multiforme (GBM) is one of the deadliest forms of human brain tumors. The infiltrative pattern of growth of these tumors includes the spread of individual and/or clusters of tumor cells at some distance from the main tumor mass in parts of the brain protected by an intact blood-brain-barrier. Pathophysiological studies of GBM could be greatly enhanced by analytical techniques capable of *in situ* single-cell resolution measurements of infiltrating tumor cells. Magnesium homeostasis is an area of active investigation in high grade gliomas. In the present study, we have used the F98 rat glioma as a model of human GBM and an elemental/isotopic imaging technique of secondary ion mass spectrometry (SIMS), a CAMECA IMS-3f ion microscope, for studying Mg distributions with single-cell resolution in freeze-dried brain tissue cryosections. Quantitative observations were made on tumor cells in the main tumor mass, contiguous brain tissue, and infiltrating tumor cells in adjacent normal brain. The brain tissue contained a significantly lower total Mg concentration of 4.70 ± 0.93 mmol/Kg wet weight (mean ± SD) in comparison to 11.64 ± 1.96 mmol/Kg wet weight in tumor cells of the main tumor mass and 10.72 ± 1.76 mmol/Kg wet weight in infiltrating tumor cells ($p<0.05$). The nucleus of individual tumor cells contained elevated levels of bound Mg. These observations demonstrate enhanced Mg-influx and increased binding of Mg in tumor cells and provide strong support for further investigation of GBMs for altered Mg homeostasis and activation of Mg-transporting channels as possible therapeutic targets.

Keywords

Magnesium homeostasis; TRPM7; Glioblastoma multiforme; Imaging mass spectrometry; B-ZIP transcription factors; Intranuclear magnesium; Imaging of total magnesium

[*]Corresponding Author: Subhash Chandra, Ph.D., Cornell SIMS Laboratory, Department of Biomedical Engineering, Cornell University, Ithaca, NY 14853, USA. Tel. 607-255-3884; Fax 607-254-4780.

Conflict of interest

The authors report no conflict of interest

Introduction

Magnesium (Mg) is essential for normal physiological and biochemical functions of the cells. It is a co-factor for more than 300 enzymes that are specifically involved in nucleic acid synthesis and energy metabolism, protein synthesis, cell proliferation, transmembrane ion flux, calcium channel gating, muscle contraction, neuronal activity, cardiac functioning, and neurotransmitter release [1–3]. Although Mg has long been implicated with cell growth and transformation [4–6], the understanding of biochemical pathways associated with its many roles in carcinogenesis is still incomplete and is an area of active research [7–9]. Approximately 5% of intracellular Mg is found in the free ionized form (Mg^{2+}), which can potentially function as second messenger similar to Ca^{2+} [10]. Alteration in either ionized and/or bound forms of Mg may have functional consequences leading to a variety of diseases.

Recent studies have shown that ion channels can regulate many malignant features of tumor cells such as decreased differentiation and increased migratory and invasive phenotypes (11, 12]. In particular, the TRPM7 channel (transient receptor potential melastatin type 7), which is permeable to both Mg^{2+} and Ca^{2+}, has been implicated with physiological processes such as cellular Mg homeostasis [13], neurotransmitter release [14] and pathological conditions such as atrial fibrillation [15] and cerebral ischemia [16]. Furthermore, TRPM7 has been reported to play a role in the growth, proliferation, and migration of many different types of tumor cells, including retinoblastoma [17], leukemia [18], prostate cancer [19], and ductal adenocarcinoma of the pancreas [20]. The overexpression of TRPM7 in human tissues of pancreatic ductal carcinoma has been correlated with the tumor grade, Ki67 proliferative index, and patient survival [20].

In recent studies of high grade gliomas, functional TRPM7 channels were observed in the A172 human GBM cell line and cells isolated from human GBMs. The activation of TRPM7 channel has been investigated to better understand the biochemical pathways implicated in proliferation, migration, and invasion of glioma cells with special emphasis on Ca signaling [21, 22]. Since TRPM7 is permeable to both Ca^{2+} and Mg^{2+} ions, and is inhibited by elevated intracellular Mg^{2+} and Mg.ATP, it has been difficult to distinguish the roles of both ions in physiological and pathological conditions associated with the function of these channels [8, 23]. This is further complicated by the fact that in most studies little attention has been given to the measurement of the total pool of Mg on a single-cell resolution basis, which may more accurately reflect alterations in cellular Mg homeostasis in pathological conditions. Such measurements are particularly important for high grade gliomas, which have an overall median survival time of approximately 15 months after diagnosis [24]. Even maximal surgical resection cannot remove infiltrating tumor cells that invade normal brain at varying distances from the main tumor mass. These infiltrating tumor cells are responsible for the regrowth of the tumor and its subsequent recurrence [25]. Therefore, single-cell resolution measurements of the total pool of Mg in infiltrating tumor cells in comparison to the normal brain tissue could provide a valuable tool for assessing alterations in Mg homeostasis of GBM cells.

In situ single-cell resolution measurements of total Mg in tissue specimens can be achieved via high vacuum techniques such as the electron probe [26] and imaging secondary ion mass spectrometry (SIMS) [27]. SIMS has a distinct advantage for single-cell resolution studies of Mg, since it can detect parts-per-million concentrations in the imaging mode [28]. In the present study, we have used the F98 rat glioma model [29] of GBM for SIMS imaging evaluation of Mg distribution with single-cell resolution in cryogenically prepared tissue sections. Our observations have demonstrated that infiltrating tumor cells in brain, as well as those in the main tumor mass, contained approximately a twofold increase in Mg concentrations compared to surrounding brain tissue. These observations provide strong support for further investigation of GBMs for alterations in Mg homeostasis.

Materials and Methods

The F98 rat glioma model and sample preparation for histological evaluation and SIMS analysis

All of the animal studies were carried out in strict accordance with the recommendations in the *Guide for the Care and Use of Laboratory Animals* of the National Institutes of Health under approved protocol by the Institutional Animal Care and Use Committee of The Ohio State University (IACUC protocol # 2007A0261-R1). The F98 rat glioma (#CRL-2397, American Type Culture Collection, Manasus, VA) has been used in a wide variety of studies in experimental neuro-oncology [29]. Its biological behavior and low immunogenicity resemble that of human high grade gliomas. As described elsewhere [29], the F98 glioma is composed of a mixed population of spindle-shaped cells, the majority of which have fusiform nuclei, and a smaller number of polygonal cells with round or oval nuclei. The tumor extensively invades contiguous normal brain and island of tumor cells can be seen at varying distances from the main tumor mass, many of which form perivascular clusters. These properties are best appreciated in permanent, paraffin embedded sections [29], rather than the frozen sections used in this study.

Male Fisher 344 rats (Charles River Laboratories, Inc., Wilmington, MA) weighing ~200 g were used in the study. F98 glioma cells (10^4) were implanted stereotactically into the right caudate nucleus of syngeneic Fisher rats. The tissue sampling was performed ~12 days following implantation. The rats were anesthetized using isoflurane and euthanized. The brains were removed and the tumors and surrounding brain tissue samples were frozen in the vapor phase of liquid nitrogen for SIMS analysis to determine Mg distribution with single-cell resolution. Approximately 4 μm thick cryosections were used for optical and SIMS imaging analysis. Sections for histological examination were mounted on glass slides and stained with hematoxylin and eosin (H & E). Cryosections for SIMS analysis were sectioned at −20 to −30 °C and attached to silicon wafers (~1 cm^2), which were then freeze-dried and sputter coated with a 10 Å layer of Au/Pd for enhancing their electrical conductivity for SIMS imaging analyses [30].

SIMS imaging analysis and quantification of Mg distribution in brain tumor and surrounding brain tissue at single-cell resolution

A CAMECA IMS-3f dynamic SIMS ion microscope instrument was used in this study (CAMECA, France). This instrument was capable of producing isotopic images revealing gradients of any elements from H to U with a lateral resolution of 500 nm [28]. Since the analysis in this type of dynamic SIMS instrument is made by gradually sputtering (eroding) the tissue sample, via primary ion beam bombardment, it is possible to record images of any number of desired elements from the same region of the sample. The spatial resolution of 500 nm was capable of imaging single tumor cells with subcellular details, including nuclei of individual cells in brain tumor tissues. Over the course of its use, the SIMS instrument was upgraded with a primary beam mass filter and a 5f Hall Probe control chassis. The control systems of the instrument were also upgraded with a Charles Evans and Associates model PC-1CS Computer Interface system and Windows-based computer. In the present study, the instrument was operated in the positive secondary ion imaging mode with samples biased to +4500 V. An O_2^+ primary ion beam, accelerated to 10 keV, was focused and adjusted to a nominal beam current of 150–200 nA with a diameter of ~70 μm when viewed as a stationary spot at the surface of the sample. The 400-μm transfer optics, in conjunction with a 60-μm contrast aperture, was employed for SIMS imaging analyses. The energy window of the mass spectrometer was centered and set to a maximal value of 130 eV. Energy and mass filtered secondary ion images were magnified and projected on a single microchannel plate/phosphor screen detection assembly. The gain of the microchannel plate was set at 60% of the maximum. SIMS ion images were recorded from the image detection assembly using a Photometrics CCD CoolSNAP HQ^2 FireWire Digital Camera capable of 14 bits/pixel image digitization. The image data was transferred from the camera controller to the PC workstation with a Nikon NIS-Elements Imaging Software for storage and digital image processing (Princeton Digital Corp., USA). The camera was operated in the 2 × 2 binning mode. In the positive secondary ion detection mode, images of isotopes with masses 12, 23, 24, 39, and 40 revealed the subcellular distribution of positive secondary ions of ^{12}C, ^{23}Na, ^{24}Mg, ^{39}K, and ^{40}Ca, respectively. High mass resolution analyses confirmed that mass interferences originating from polyatomic ions and cell matrix components were negligible, which is in agreement with our previous studies of Mg analysis by dynamic SIMS [31, 32]. The pixel-by-pixel image quantification of $^{24}Mg^+$ signals was achieved by using $^{12}C^+$ carbon normalization approach and the relative-sensitivity-factors (RSF) of $^{24}Mg^+$ to the $^{12}C^+$ tissue matrix signals in the same spatial registration [27, 33]. This image quantification approach corrected for any variations in primary beam density on the sample surface and $^{24}Mg^+$ signal variations in raw SIMS images due to inhomogeneous microchannel plate response [33]. The Mg concentrations produced from SIMS images of freeze-dried tissues were converted into estimated wet weight concentrations by assuming 85% water content of tissues.

Statistical analysis

A Minitab Statistical Software was used for statistical analysis of the data using ANOVA. A *p* value of less than 0.05 was considered significant.

Results

The F98 rat glioma provided an ideal model for SIMS imaging studies of Mg distribution in the main tumor mass, which has an altered blood-brain-barrier (BBB), normal brain tissue, and infiltrating tumor cells in the brain, which are protected by an intact BBB. In the F98 rat glioma model, tumor cells almost invariably infiltrate normal brain as individual cells or as clusters of cells together, referred to here as the tumor satellites. Examples of single-cell resolution SIMS imaging analyses of Mg distribution in F98 rat glioma are shown in Figs. 1–3 and the details of each figure are discussed below.

An example of SIMS analysis of the main tumor mass of the F98 rat glioma is shown in Fig. 1. The optical image of a H & E stained cryosection illustrates the high density of tumor cells in the main tumor mass with discernible nuclei (N) of individual cells (Panel A, Fig. 1). SIMS imaging analysis of the main tumor mass from an adjacent cryosection revealed the spatial distribution of total concentrations of ^{24}Mg and ^{40}Ca in positive secondary ion SIMS images (Panels B & C, Fig. 1). Since the level of brightness within a SIMS image is directly proportional to the relative ion intensities, the nuclei (N) of tumor cells are discernible in the ^{24}Mg SIMS ion image (Fig. 1B). In contrast, the ^{40}Ca distribution reveals lower intensities from nuclear regions, in general, and a few high intensity precipitates of Ca are plausibly from apoptotic and dead cells (Fig. 1C). Furthermore, since SIMS images are recorded by the gradual sputtering (erosion) of the sample surface from an adjacent cryosection, a direct correlation of the density of nuclei between the optical and the $^{24}Mg^+$ SIMS image cannot be made. It should be noted that in the optical image the density of nuclei reflects the entire 4 μm thickness of the tissue section. However, the SIMS $^{24}Mg^+$ image only reflects the removal of approximately 0.2 μm slice of the tissue section eroded for the recording of the image. The $^{39}K/^{23}Na$ ratio from SIMS analyses of these tissues ranged from 4–9, which is indicative of the lack of a gross redistribution of diffusible elements during the sample preparation. It should be noted that intracellular total Mg distribution is much less prone to diffusion artifacts in cryogenic sample preparation due to the fact that the majority of Mg in the cell is present in a bound form to molecules and the gradient of free Mg^{2+} between the extracellular and intracellular *milieu* is minimal in comparison to other major physiologically relevant cations like Ca^{2+}, K^+, and Na^+. It should also be noted that in raw SIMS images, as shown here, the slight dimming of the secondary ion signals towards the center of SIMS images is due to a typical inhomogeneous response of the microchannel plate. This inhomogeneous response is accounted for and corrected in quantitative analysis by SIMS image quantification approach used in this study and discussed in methods section.

Figure 2 shows an example of SIMS analysis of Mg distribution in a tissue section containing a portion of the tumor mass and surrounding brain tissue with infiltrating tumor cells. The optical image from a H & E stained cryosection (Panel A, Fig. 2) illustrates a portion of the tumor mass (TM) and adjacent brain tissue (BT) containing individual infiltrating tumor cells (TC). SIMS imaging analysis from an adjacent cryosection revealed a clear gradient in the ^{24}Mg distribution with higher intensities in the main tumor mass in comparison to the adjacent brain tissue (Panel B, Fig. 2). Furthermore, the individual infiltrating tumor cells (TC) in the brain tissue contained higher levels of Mg compared to

the surrounding brain tissue (Panel B, Fig. 2). A vessel (V), surrounded by individual tumor cells, is also discernible in the brain tissue region of the ^{24}Mg SIMS image. The SIMS image of carbon (^{12}C) from the same tissue region shows a near homogeneous distribution of carbon between the tumor mass and the brain tissue and an obvious lack of carbon matrix inside the vessel area (Panel C, Fig. 2). The ^{12}C carbon image is used for pixel-by-pixel registration and quantification of ^{24}Mg SIMS images (see quantitative analysis later).

Infiltrating F98 glioma cells may spread in the brain as individual tumor cells, which can proliferate to form clusters of tumor cells constituting tumor satellites. Examples of SIMS analyses of Mg distribution in brain tissue regions containing tumor satellites are shown in Fig. 3. Histological images of H & E stained cryosections illustrate a tumor satellite (TS) of approximately 60 μm in the diameter in the brain tissue (Panel A, Fig. 3) and a vessel (V) surrounded by individual tumor cells in the brain tissue (Panel B, Fig. 3). This pattern of tumor cell infiltration of the brain tissue to form satellite tumors in the F98 glioma are common features of human GBMs. SIMS imaging of ^{24}Mg distribution from two different cryosections containing such regions are shown in Fig. 3 (panels C & D). These observations unequivocally demonstrated gradients of higher Mg in tumor satellites (TS) and individual infiltrating tumor cells in comparison to the surrounding brain tissue.

Quantitative measurements of total Mg concentrations in the brain tissue, tumor cells in main tumor mass, and infiltrating tumor cells in the brain, including single tumor cells and tumor satellites, are listed in Table 1. The F98 tumor cells contained significantly higher ($p<0.05$) concentrations of total Mg than the brain tissue. Furthermore, there was no significant difference in total Mg concentrations in tumor cells of the main tumor mass and infiltrating tumor cells in normal brain (Table 1). These observations indicate that infiltrating F98 glioma cells, invading as single cells, can proliferate to form clusters or satellites, and maintain their higher levels of total Mg concentrations irrespective of the fact that they are at varying distances from the main tumor mass.

Discussion

The ideal assessment of alterations in Mg homeostasis in carcinogenesis would require *in vivo* single-cell resolution measurements of both free Mg^{2+} and total Mg concentrations in normal and tumor tissues. However, no single technique is currently capable of providing these two measurements *in vivo*. Although SIMS cannot be applied to live cell imaging studies due to its high vacuum conditions, the use of cryogenically-fixed samples provides an effective *in situ* measurement of total Mg concentrations.

The present study adds valuable SIMS methodology for the assessment of Mg homeostasis, based on single-cell resolution quantitative imaging of total Mg in tissue sections. This could be particularly useful for evaluating high grade gliomas, where infiltration of tumor cells into surrounding normal brain results in regrowth after surgical resection of the main tumor mass. Single-cell resolution measurements provide an improvement over conventional methods of total Mg determination in tumor versus normal tissues via techniques such as atomic absorption spectroscopy, since homogenization of the tumors would result in mixing of both necrotic and viable portions of the tumor, as well as

infiltrating non-neoplastic cells and extracellular fluids, thereby producing inaccuracies in the measurements. Indeed, inconsistent and often contradictory observations of decreased or increased levels of Mg in various types of cancers have been reported based on tissue homogenization methods [34, 35]. Nevertheless, these early studies were valuable in demonstrating that all cancers cannot be grouped under one category and each type should be regarded as a separate entity for the regulation of metal concentrations.

The higher concentrations of total Mg in F98 glioma cells observed in our study (Table 1) complement a previous MRI study in which elevated levels of intracellular free Mg^{2+} were reported in brain tumors in comparison to the normal brain tissue [36]. Although infiltrating tumor cells could not be resolved in the MRI study, it provided an invaluable *in vivo* observation on the possibility of alterations in Mg homeostasis in brain tumors. It should be noted that free intracellular Mg^{2+}, which has been estimated to be in the range of 0.2–0.6 mM in human and rodent brain tissues [36–38], only represents a small fraction of the total Mg in cells. Our observations that tumor cells contained approximately twice the concentration of total Mg compared to normal brain tissue (~11 Vs 5 mmol/Kg wet weight, Table 1) indicate the presence of a much larger pool of bound Mg in tumors than can be reflected only in the increase of free Mg^{2+} species. It is also apparent from our correlative optical and SIMS analyses that the nuclei of brain tumor cells are the main contributing structure for enhanced binding of Mg (Figs. 1–3). Increased binding of Mg in the nucleus was previously reported in human thyroid tumor cells based on the analysis of tissue cryosections with the electron microprobe [39].

Intracellular Mg binding plays key roles in stabilizing protein structures and negatively charged phosphate groups of nucleic acids [40]. Alterations in intranuclear Mg concentrations may have profound effects on the sequence specific DNA binding of basic leucine zipper (B-ZIP) transcription factors and regulation of gene expression, as observed in model systems in *in vitro* studies [41, 42]. The B-ZIP transcription factors mediate a variety of signaling pathways and certain types of B-ZIP proteins have been identified as molecular targets of various diseases, including diabetes and cancer [43, 44]. The expression of B-ZIP transcription factor ATF5 was detected in human GBMs and rat glioma cell lines [45]. Another role of intranuclear bound Mg may involve in affecting the structure of DNA itself. At higher concentrations there is an accumulation of Mg binding, which induces non-B-DNA structures like the Z-DNA [46]. The understanding of biological roles of non-B-DNA structures in carcinogenesis is an area of active study [47–50].

The present study revealed that infiltrating tumor cells and cells in the main tumor mass showed comparable increases of total Mg compared to Mg concentration of the normal brain tissue. This was a very significant observation, since it indicated the inherent nature of alterations in Mg transport as a characteristic of individual tumor cells (Figs. 2 and 3, Table 1). Due to the very high sensitivity of SIMS and the capability to simultaneously sampling a large field of view, these images of Mg distribution were obtained within one minute integration of ^{24}Mg signals (Figs. 1–3). Such a capability is a major strength of SIMS for unraveling the possible roles of Mg in cancer, and more specifically, high grade gliomas.

The twofold increase in total Mg in brain tumor cells observed in our study may have been due to higher metabolic activity and activation of Mg^{2+} and Ca^{2+} transporting channels like TRPM7 and CNNM3, as observed in various cancers [7–9]. There is growing interest in understanding the role of TRPM7 overexpression and biochemical pathways implicated with proliferation, migration, and invasion of many types of cancers such as retinoblastoma [17], leukemia [18], prostate [19], and adenocarcinoma [20]. Most recently, high grade gliomas have been investigated for the overexpression of TRPM7 with special emphasis on calcium signaling [21, 22]. The present study suggests that any evaluation of TRPM7 should also include the understanding of pathological roles of elevated levels of bound Mg in high grade gliomas.

Acknowledgments

This study was funded by a NIH grant 5R01 CA129326 (SC, RFB). Susan C. Pannullo, M.D. is acknowledged for providing partial funding for the completion of this project. We thank Dr. Weilian Yang for carrying out tumor cell implantations of the F98 glioma. The use of Cornell Microscopy and Imaging Facility (MIF), Department of Biomedical Engineering, is gratefully acknowledged during the study. Cornell SIMS Laboratory (S. Chandra, Principal Investigator) was affiliated with New York State Foundation for Science, Technology, and Innovation (NYSTAR).

References

1. Bara M, Guiet-Bara A, Durlach J. Regulation of sodium and potassium pathways by magnesium in cell membranes. Magnes Res. 1993; 6:167–177. [PubMed: 8274363]
2. Wolf FI, Fasanella S, Tedesco V, Torsello A, Sgambato A, Faraglia B, Faraglia B, Palozza P, Boninsegna A, Cittadini A. Regulation of magnesium content during proliferation of mammary epithelial cells (HC-11). Front Biosci. 2004; 9:2056–2062. [PubMed: 15353270]
3. Jahnen-Dechent W, Ketteler M. Magnesium basics. Clin Kidney J. 2012; 5(Suppl 1):i3–i14. [PubMed: 26069819]
4. Anghileri LJ. Calcium, magnesium, and phosphorus in experimental tumors: Effects of the age of the tumors. Z Krebsforsch. 1974; 81:109–119.
5. McKeehan WL, Ham RG. Calcium and magnesium ions in the regulation of multiplication in normal and transformed cells. Nature. 1978; 275:756–758. [PubMed: 212683]
6. Rubin H. Central roles of Mg^{2+} and $Mg.ATP^{2-}$ in the regulation of protein synthesis and cell proliferation: significance for neoplastic transformation. Adv Cancer Res. 2005; 93:1–58. [PubMed: 15797443]
7. Castiglioni S, Maier JAM. Magnesium and cancer: a dangerous liaison. Magnes Res. 2011; 24:S92–S100. [PubMed: 21933757]
8. Wolf FI, Trapani V. Magnesium and its transporters in cancer: a novel paradigm in tumor development. Clin Sci. 2012; 123:417–427. [PubMed: 22671428]
9. Hardy S, Uetani N, Wong N, Kostantin E, Labbe DP, Bégin LR, Mes-Masson A, Miranda-Saavedra D, Tremblay ML. The protein tyrosine phosphatase PRL-2 interacts with the magnesium transporter CNNM3 to promote oncogenesis. Oncogene. 2015; 34:986–995. [PubMed: 24632616]
10. Feske S, Skolnik EY, Prakriya M. Ion channels and transporters in lymphocyte function and immunity. Nat Rev Immunol. 2012; 12:532–547. [PubMed: 22699833]
11. Lehen'kyi V, Shapovalov G, Skyrma R, Prevarskaya N. Ion channels and transporters in cancer. 5. Ion channels in control of cancer and cell apoptosis. Am J Physiol Cell Physiol. 2011; 301:C1281–C1289. [PubMed: 21940667]
12. Trapani V, Arduini D, Cittadini A, Wolf FI. From magnesium to magnesium transporters in cancer: TRPM7, a novel signature in tumor development. Magnes Res. 2013; 26:149–155. [PubMed: 24556627]

13. Schmitz C, Perraud A-L, Johnson CO, Inabe K, Smith MK, Penner R, Kurosaki T, Fleig A, Scharenberg AM. Regulation of vertebrate cellular Mg^{2+} homeostasis by TRPM7. Cell. 2003; 114:191–200. [PubMed: 12887921]

14. Krapivinski G, Mochida S, Krapivinski L, Cibulsky SM, Clapham DE. The TRPM7 ion channel functions in cholinergic synaptic vesicles and affects transmitter release. Neuron. 2006; 52:485–496. [PubMed: 17088214]

15. Du J, Xie J, Zhang Z, Tsujikawa H, Fusco D, Silverman D, Liang B, Yue L. TRPM7-mediated Ca^{2+} signals confer fibrogenesis in human atrial fibrillation. Circ Res. 2006; 106:992–1003. [PubMed: 20075334]

16. Leng T, Shi Y, Xiong Z-G, Sun D. Proton-sensitive cation channels and ion exchangers in ischemic brain injury: New therapeutic agents for stroke? Prog Neurobiol. 2014; 115:189–209. [PubMed: 24467911]

17. Hanano T, Hara Y, Shi J, Morita H, Umebayashi E, Mori H, Sumimoto Y, Ito Y, Mori R, Inoue J. Involvement of TRPM7 in cell growth as a spontaneously activated Ca^{2+} entry pathway in human retinoblastoma cells. J Pharmacol Sci. 2004; 95:403–419. [PubMed: 15286426]

18. Zierler S, Yao G, Zhang Z, Kuo WC, Porzgen P, Penner R, Horgen FD, Fleig A. Waixenicin A inhibits cell proliferation through magnesium-dependent block of transient receptor potential melastatin 7 (TRPM7) channels. J Biol Chem. 2011; 286:39328–39335. [PubMed: 21926172]

19. Sun Y, Selvaraj S, Verma A, Derry S, Sahmoun AE, Singh BB. Increase in serum Ca^{2+}/Mg^{2+} ratio promotes proliferation of prostate cancer cells by activating TRPM7 channels. J Biol Chem. 2013; 288:255–263. [PubMed: 23168410]

20. Rybarczyk P, Gautier M, Hague F, Dhennin-Duthille I, Chatelain D, Kerr-Conte J, Pattou F, Regimbeau J-M, Sevestre H, Ouadid-Ahidouch H. Transient receptor potential melastatin-related 7 channel is overexpressed in human pancreatic ductal adenocarcinomas and regulates human pancreatic cancer cell migration. Int J Cancer. 2012; 131:E851–E861. [PubMed: 22323115]

21. Liu M, Inoue K, Leng T, Guo S, Xiong Z-G. TRPM7 channels regulate glioma stem cell through STAT3 and NOTCH signaling pathways. Cellular Signal. 2014; 26:2773–2781.

22. Leng T-D, Li M-H, Shen JF, Liu M-L, Li X-B, Sun H-W, Braningan D, Zeng Z, Si H-F, Li J, Chen J, Xiong Z-G. Supression of TRPM7 inhibits proliferation, migration, and invasion of malignant human glioma cells. CNS Neurosci Ther. 2015; 21:252–261. [PubMed: 25438992]

23. Ryazanova LV, Rondon LJ, Zierler S, Hu Z, Galli J, Yamaguchi TP, Mazur A, Fleig A, Ryazanov AG. TRPM7 is essential for Mg^{2+} homeostasis in mammals. Nat Commun. 2010; 1:109.10.1038/ncomms1108 [PubMed: 21045827]

24. Stupp R, Hegi ME, Mason WP, van den Bent MJ, Taphoorn MJ, Janzer RC, et al. Effects of radiotherapy with concomitant and adjuvant temozolomide versus radiotherapy alone on survival in glioblastoma in a randomized Phase III study: 5-year analysis of the EORTC-NCIC trial. Lancet Oncol. 2009; 10:459–466. [PubMed: 19269895]

25. Burger PC, Dubois PJ, Schold SC Jr, Smith KR Jr, Odom GL, Crafts DC, Giangaspero F. Computerized tomographic and pathologic studies of the untreated, quiescent, and recurrent glioblastoma multiforme. J Neurosurg. 1983; 58:159–169. [PubMed: 6294260]

26. De Francesco A, Desnoyer RW, Covacci V, Wolf FI, Romani A, Cittadini A, Bond M. Changes in magnesium content and subcellular distribution during retinoic acid-induced differentiation of HL 60 cells. Arch Biochem Biophys. 1998; 360:149–157. [PubMed: 9851825]

27. Chandra S, Morrison GH, Beyenbach KW. Identification of Mg-transporting renal tubules and cells by ion microscopy imaging of stable isotopes. Am J Physiol. 1997; 273:F939–F948. Renal Physiol. 42. [PubMed: 9435683]

28. Chandra S, Smith DR, Morrison GH. Subcellular imaging by dynamic SIMS ion microscopy. Anal Chem. 2000; 72:104A–114A.

29. Barth RF, Kaur B. Rat brain tumor models in experimental neuro-oncology: the C6, 9L, T9, RG2, F98, BT4C, RT2, and CNS-1 gliomas. J Neurooncol. 2009; 94:299–312. [PubMed: 19381449]

30. Smith DR, Chandra S, Barth RF, Yang W, Joel DD, Coderre JA. Quantitative imaging and microlocalization of boron-10 in brain tumors and infiltrating tumor cells by SIMS ion microscopy: Relevance to neutron capture therapy. Cancer Res. 2001; 61:8179–8187. [PubMed: 11719448]

31. Chandra S, Ausserer WA, Morrison GH. Evaluation of matrix effects in ion microscopic analysis of freeze-fractured, freeze-dried cultured cells. J Microsc. 1987; 148:223–239. [PubMed: 3443979]
32. Chandra S, Morrison GH. Evaluation of ^{26}Mg stable isotope as a tracer of magnesium transport for SIMS ion microscopy imaging studies. J Microsc. 1997; 188:182–190. [PubMed: 9418273]
33. Ausserer WA, Ling Y-C, Chandra S, Morrison GH. Quantitative imaging of boron, calcium, magnesium, potassium, and sodium in cultured cells. Anal Chem. 1989; 61:2690–2695. [PubMed: 2619055]
34. Mulay IL, Roy R, Knox BE, Suhr NH, Delaney WE. Trace-metal analysis of cancerous and noncancerous human tissues. J Natl Cancer Inst. 1971; 47:1–13. [PubMed: 4328191]
35. Rande SS, Panday VK. Major metals in human cancer: calcium, magnesium, sodium and Potassium. Sci Total Environ. 1985; 41:79–89. [PubMed: 3969548]
36. Taylor JS, Vigneron DB, Murphy-Boesch J, Nelson SJ, Kessler HB, Coia L, Curran W, Brown TR. Free magnesium levels in normal human brain and brain tumors: ^{31}P chemical-shift imaging measurements at 1.5 T. Proc Natl Acad Sci USA. 1991; 88:6810–6814. [PubMed: 1650484]
37. Voloso D, Guynn RW, Oskarsson M, Veech RL. The concentrations of free and bound magnesium in rat tissues. J Biol Chem. 1973; 248:4811–4819. [PubMed: 4718747]
38. Iotti, S.; Malucelli, E. Free magnesium concentration in the human brain. In: Vink, Robert; Nechifor, Mihai, editors. Magnesium in the central nervous system. University of Adelaide Press, Barr Smith Library, The University of Adelaide; South Australia: 2011. p. 3-12.
39. Lukács GL, Zs-Nagy I, Steiber J, Györi F, Balázs Z. Relative intranuclear magnesium and phosphorus contents in normal and tumor cells of the human thyroid gland as revealed by energy-dispersive X-ray microanalysis. Scanning Microsc. 1996; 10:191–200.
40. Piovesan D, Profiti G, Martelli PL, Casadio R. The human “magnesome”: detecting magnesium binding sites on human proteins. BMC Bioinformatics. 2012; 13(Suppl 14):S10.10.1186/1471-2105-13-S14-S10 [PubMed: 23095498]
41. Craig JC, Schumacher MA, Mansoor SE, Farrens DL, Brennan RG, Goodman RH. Consensus and variant cAMP-regulated enhancers have distinct CREB binding properties. J Biol Chem. 2001; 276:11719–11728. [PubMed: 11134034]
42. Moll JR, Acharya A, Gal J, Mir AA, Vinson C. Magnesium is required for specific DNA binding of the CREB B-ZIP domain. Nucleic Acids Res. 2002; 30:1240–1246. [PubMed: 11861917]
43. Zhu S, Yoon K, Sterneck E, Johnson PF, Smart RC. CCAAT/Enhancer binding protein beta is a mediator of keratinocyte survival and skin tumorigenesis involving oncogenic Ras signaling. Proc Natl Acad Sci USA. 2002; 99:207–212. [PubMed: 11756662]
44. Rishi V, Potter T, Laudeman J, Reinhart R, Silvers T, Selby M, Stevenson T, Krosky P, Stephen AG, Acharya A, Moll J, Oh WJ, Scudiero D, Shoemaker RH, Vinson CA. High-throughput fluorescence-anisotropy screen that identifies small molecule inhibitors of the DNA binding of B-ZIP transcription factors. Anal Biochem. 2005; 340:259–271. [PubMed: 15840499]
45. Angelastro JM, Canoll PD, Kuo J, Weicker M, Costa A, Bruce JN, Greene LA. Selective destruction of glioblastoma cells by interference with the activity of expression of ATF5. Oncogene. 2006; 25:907–916. [PubMed: 16170340]
46. Anastassopoulou J, Theophanides T. Magnesium-DNA interactions and the possible relation of magnesium to carcinogenesis. Irradiation and free radicals. Crit Rev Oncol Hematol. 2002; 42:79–91. [PubMed: 11923070]
47. Dobi A, Agoston DV. Submillimolar levels of calcium regulate DNA structure at the dinucleotide repeat $(TG/AC)_n$. Proc Natl Acad Sci USA. 1998; 95:5981–5986. [PubMed: 9600903]
48. Rich A, Zhang S. Z-DNA: the long road to biological function. Nat Rev Genet. 2003; 4:566–572. [PubMed: 12838348]
49. Wang G, Christensen LA, Vasquez KM. Z-DNA forming sequences generate large-scale deletions in mammalian cells. Proc Natl Acad Sci USA. 2006; 103:2677–2682. [PubMed: 16473937]
50. Ray BK, Dhar S, Henry C, Rich A, Ray A. Epigenetic regulation by Z-DNA silencer function controls cancer associated ADAM-12 expression in breast cancer: cross-talk between MeCP2 and NF1 transcription factor family. Cancer Res. 2013; 73:736–744. [PubMed: 23135915]

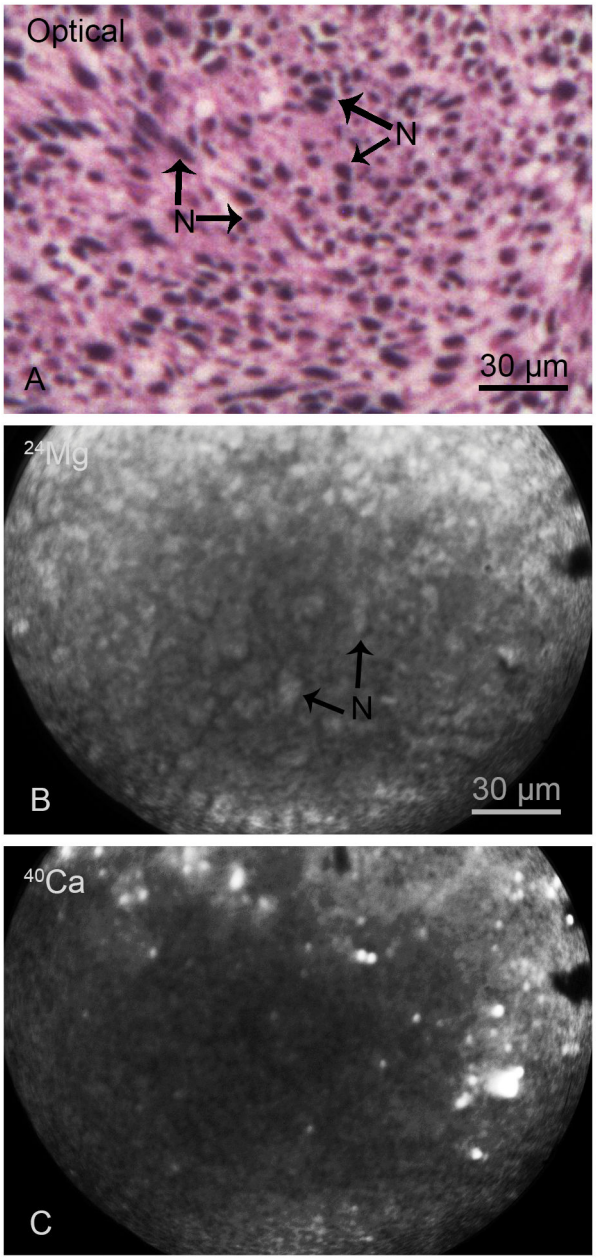

Fig. 1.

SIMS imaging of total Mg and Ca distributions in the main tumor mass of a F98 glioma bearing rat. The optical image of a H & E stained cryosection illustrates nuclei (N) of individual cells compacted in the tumor mass (A). The positive secondary ion SIMS images of ^{24}Mg and ^{40}Ca from an adjacent cryosection demonstrate the spatial distribution of total magnesium and calcium in the tumor mass (B, C). The image integration times on the CCD camera for SIMS images of $^{24}Mg^{+}$ and $^{40}Ca^{+}$ were 1 min and 2 min, respectively.

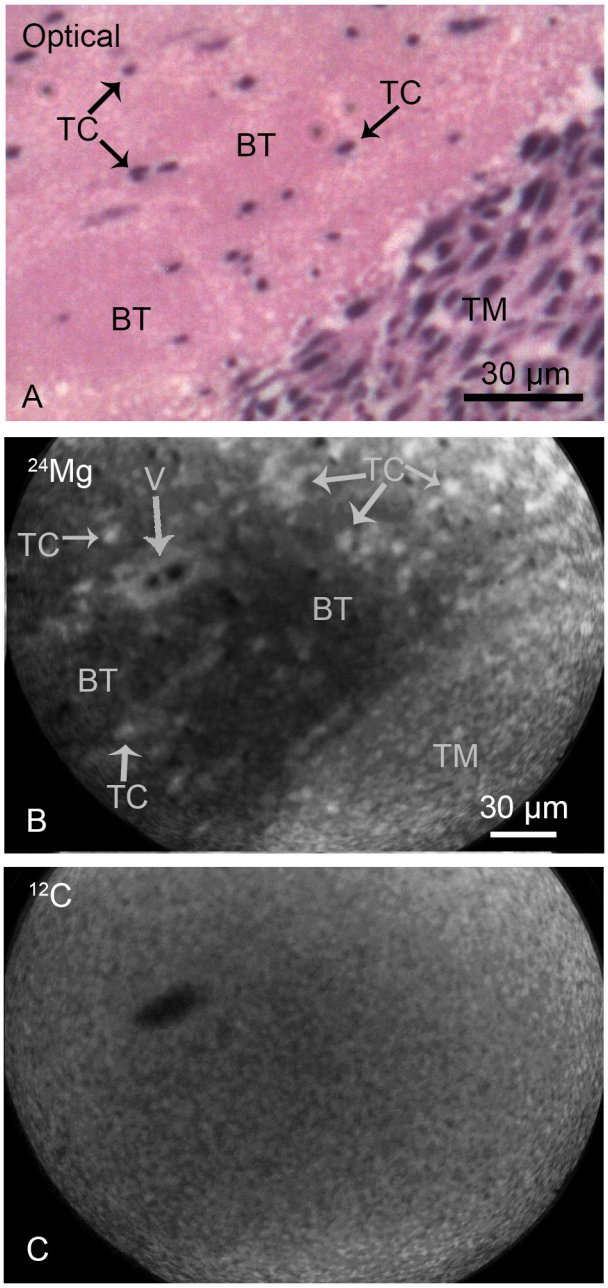

Fig. 2.

SIMS imaging of magnesium and carbon distributions from the brain of a F98 glioma bearing rat. The optical image of a H & E stained cryosection (panel A) illustrates the interface between the tumor mass (TM) and the brain tissue (BT) with infiltrating individual tumor cells (TC). The positive secondary ion SIMS images of ^{24}Mg and ^{12}C from an adjacent cryosection demonstrate the spatial distribution of total magnesium and carbon in designated panels (B, C). The tumor mass as well as infiltrating tumor cells in the brain tissue show higher concentrations of magnesium in comparison to the surrounding brain tissue (B). A vessel (V) is also discernible in the ^{24}Mg image. The ^{12}C SIMS image reveals a near homogeneous distribution of carbon throughout the tumor mass and the brain tissue

with the exception of the interior of the vessel which lacks the carbon matrix (C). The image integration times on the CCD camera for SIMS images of $^{24}Mg^{+}$ and $^{12}C^{+}$ were 1 min and 2 min, respectively.

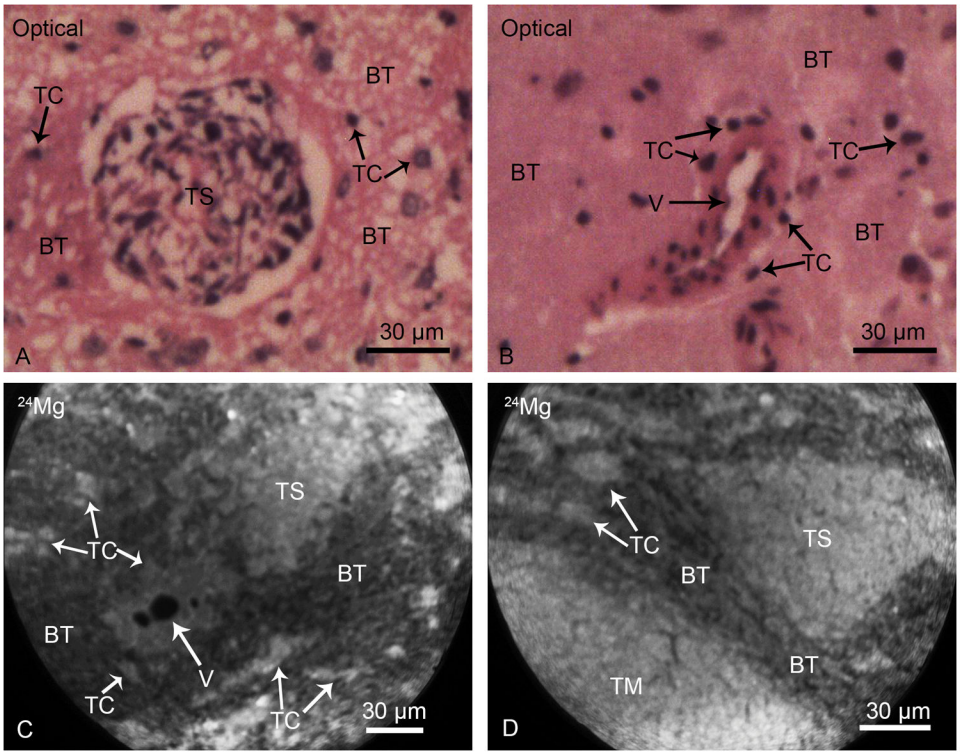

Fig. 3.

SIMS analyses of brain from F98 glioma bearing rats. Typical morphological features of infiltrating tumor cells (TC) and clusters of tumor cells, tumor satellites (TS), in the brain tissue (BT) are illustrated in optical images of H & E stained cryosections (Panels A & B). A vessel (V) is surrounded by infiltrating tumor cells in the brain tissue (Panel B). SIMS imaging analysis of ^{24}Mg distributions from two different cryosections are shown in panels C and D. The tumor satellites (TS), infiltrating tumor cells (TC) and TC's surrounding the vessel (V) reveal higher total magnesium concentrations in comparison to the surrounding brain tissue (BT). The ^{24}Mg SIMS image, shown in the panel D, also illustrates a portion of the tumor mass (TM) alongside of a triangular tumor satellite region in the brain tissue with consistent observations of higher magnesium concentrations in tumor mass, tumor satellites, and individual infiltrating tumor cells in comparison to the brain tissue. The image integration times on the CCD camera for $^{24}Mg^{+}$ SIMS images were 1 min each.

Table 1

Quantitative SIMS imaging analysis of total magnesium concentrations in F98 rat glioma brain regions. Total Mg concentrations are expressed in mmol/Kg wet weight units by assuming 85% tissue water content. The spatially-resolved observations were pooled from quantitative SIMS imaging analysis of tissues from five F98 glioma bearing rats.

Brain Tissue Regions[a]	Total Mg Concentration (mmol/Kg wet weight) (mean ± SD)
Normal brain tissue	4.70 ± 0.93[b]
Tumor cells in the main tumor mass	11.64 ± 1.96[c]
Infiltrating tumor cells in the brain tissue	10.72 ± 1.76[c]

[a]For sampling of tumor cells in the main tumor mass from $^{24}Mg^{+}$ SIMS images, 107 regions of interest (ROIs) in the main tumor mass were selected from 6 SIMS imaging fields. A region of interest in the magnesium image of the main tumor mass was defined as a clump of 5–10 individual cells taken together for SIMS image quantification due to very high density of tumor cells in this region. This approach allowed a large sampling of the cells in the main tumor mass. For sampling of infiltrating tumor cells in the brain tissue of $^{24}Mg^{+}$ SIMS images, 115 ROIs were selected containing individual tumor cells and cells in the tumor satellite regions from 5 SIMS imaging fields. The sampling of brain tissue regions represented 108 ROIs of 10–15 μm^2 area from 6 SIMS imaging fields.

[b,c]Total Mg concentrations in tumor cells in the main tumor mass and infiltrating tumor cells in the brain were significantly ($p<0.05$) higher than Mg concentration of the brain tissue. The Mg concentration of tumor cells in the main tumor mass was not significantly different from the infiltrating tumor cells in the brain.